J. Fluid Mech. (1977), *vol.* 79, *part* 1, *pp.* 49–69
Printed in Great Britain

Hydromechanics of lunate-tail swimming propulsion. Part 2

By M. G. CHOPRA† AND T. KAMBE‡
Department of Applied Mathematics and Theoretical Physics, University of Cambridge

(Received 16 January 1976)

This paper investigates the propulsive performance of the lunate tails of aquatic animals achieving high propulsive efficiency (the hydromechanical efficiency being defined as the ratio of the work done by the mean forward thrust to the mean rate at which work is done by the tail movements on the surrounding fluid). Small amplitude heaving and pitching motions of a finite flat-plate wing of general planform with a rounded leading edge and a sharp trailing edge are considered. This is a generalization of Chopra's (1974) work on model rectangular tails. This motion characterizes vertical oscillations of the horizontal tail flukes of some cetacean mammals. The same oscillations, turned through a right angle to become horizontal motions of side-slip and yaw, characterize the caudal fins of certain fast-swimming fishes; viz. wahoo, tunny, wavyback skipjack, etc., from the Percomorphi and whale shark, porbeagle, etc., from the Selachii. Davies' (1963, 1976) method of finding the loading distribution on the wing and generalized force coefficients, through approximate solution of an integral equation relating the loading and the upwash (lifting-surface theory), is used to find the total thrust and the rate of working of the tail, which in turn specify the hydromechanical swimming performance of the animals. The physical parameters concerned are the tail aspect ratio ((span)^2/planform area), the reduced frequency (angular frequency × typical length/forward speed), the feathering parameter (the ratio of the tail slope to the slope of the path of the pitching axis), the position of the pitching axis, and the curved shapes of the leading and trailing edges. The variation of the thrust and the propulsive efficiency with these parameters has been discussed to indicate the optimum shape of the tail. It is found that, compared with a rectangular tail, a curved leading edge as in lunate tails gives a reduced thrust contribution from the leading-edge suction for the same total thrust; however, a sweep angle of the leading edge exceeding about 30° leads to a marked reduction of efficiency. Another implication of the present analysis is that no negative work is involved in the actual oscillation of the tail.

The present results are used to obtain an estimate of the drag coefficient for the motion of the animals, based on observed data and the computed thrust. The results show some evidence of differences between the C_D's for cetacean mammals and scombroid fish respectively. Some discussion of this difference is also given.

† Present address: Defence Science Laboratory, Metcalfe House, Delhi, India.
‡ Present address: Department of Physics, University of Tokyo, Hongo, Bunkyo-ku, Tokyo, Japan.

1. Introduction

The continuing theme of Lighthill's (1960, 1969, 1970, 1971, 1975) and Wu's (1961, 1971*a–d*) studies of aquatic-animal locomotion is the propulsive efficiency, which is similar to the Froude efficiency of a propeller and is defined by

$$\eta = U\bar{P}/\bar{E},$$

where U is the mean forward velocity, $\bar{P}$ the mean thrust required to overcome the viscous drag of the animal and $\bar{E}$ the mean rate at which the animal is doing work against the surrounding medium. The importance of this parameter has been realized because of the impressive capability of some animals to generate surprisingly fast movements at low energy cost. This parameter depends on the propulsive mode, which, following Breder (1926), can be classified as anguilliform (an undulatory mode in which a transverse wave of increasing amplitude passes along the body from head to tail) or carangiform (a development of the anguilliform mode in which the undulations are confined to the posterior part only). The anguilliform mode, which relies heavily on the resistive forces, is found in animals swimming with relatively lower hydrodynamic efficiency; the carangiform mode relies more on the reactive forces, which can always operate more efficiently, and is found in a wide variety of fishes and other vertebrates.

It is interesting to note that all the faster marine animals (represented by teleosts such as the tunnyfishes, elasmobranchs, including the fast sharks, and most of the cetacean mammals) have evolved a similar carangiform mode of propulsion. They undulate their crescent-moon-shaped tails of large aspect ratio symmetrically about the peduncle without exhibiting any appreciable bending of their rather rigid body. The lunate tail seems to be some sort of culminating point of the process of improvement of speed and efficiency in the above-mentioned ace swimmers. Like an aeroplane wing, it possesses sections with a rounded leading edge and a sharp trailing edge, which suggests that the techniques of unsteady wing theory may be applied to study its hydromechanics. Lighthill (1970) made a start on the study of lunate-tail hydrodynamics by basing his two-dimensional analysis on the acceleration potential. Chopra (1976) developed the large amplitude theory of lunate-tail hydrodynamics (which is complementary to Lighthill's (1971) 'large amplitude elongated-body theory') and predicted that optimum swimming performance is realized with a reduced frequency around 0·8 accompanied by an amplitude as high as twice the central chord length of the lunate tail, which is in line with the carefully documented experiments of Fierstine & Walters (1968) on wavyback skipjacks.

These theories overestimate the thrust and efficiency as they account for only the spanwise wake vorticity, neglecting the streamwise component resulting from the finite span of the wing. Chopra (1974) based his three-dimensional, small amplitude, analysis of the unsteady lunate tail, for a model rectangular wing, on equations for the vorticity distribution, which he found convenient for representing the effect of the streamwise wake vorticity. The analysis gave a

clear picture of the variation of the thrust and the hydromechanical efficiency with the aspect ratio, the feathering parameter and the reduced frequency, besides the important confirmation that the pitching axis has to be approximately along the trailing edge for high efficiency.

The object of this paper is to work out a lifting-surface theory which can be applied to small amplitude motion of thin plates with general planform similar to the actual lunate tails of the fast marine animals. Heaving and pitching oscillations of the tail which maintain a constant rectilinear forward velocity U through otherwise quiescent incompressible fluid are considered. These are characteristic of the vertical motion of the tail flukes of whales and dolphins. The same oscillations turned through a right angle to become horizontal motions of side-slip and yaw characterize the motion of the caudal fins of scombroid fishes; e.g. tunny, wahoo and wavyback skipjack. The loading and moment of forces on the tail are calculated using Davies' (1963, 1976) method, which involves approximate solution of the integral equation relating the loading and the upwash. The loading and the moment readily yield the values of the thrust due to the loading, the thrust due to the leading-edge suction and the mean rate of working, which in turn specify the hydromechanical swimming performance of the animal. The thrust and the propulsive efficiency depend on (i) the tail aspect ratio, (ii) the curved shapes of the leading and trailing edges of the lunate-tail wing and (iii) the accompanying oscillatory motions specified through the reduced frequency, the feathering parameter and the position of the pitching axis. The variation of the thrust and the efficiency with these parameters has been discussed in detail to indicate the optimum shape of the tail and the accompanying undulatory motions.

It is found that, compared with rectangular tails, a curved leading edge as in the lunate tail gives a reduced thrust contribution from the leading-edge suction for the same total thrust. This is an advantage of the lunate tail since very high leading-edge suction leads to boundary-layer separation, causing considerable thrust reduction. However, a sweep angle of the leading edge exceeding about 30° leads to marked reduction of efficiency. An implication of the present analysis is that no negative work is done in the actual oscillation of the tail. Biologists have shown that a positive energy cost is incurred in the musculature not only when animals do positive work, but also when they do negative work. Hence the total work done during any cycle of oscillation including a phase of negative working would involve an additional positive energy cost, yielding an efficiency smaller than the purely hydromechanical one. This seems not to be the case for the actual motion of lunate tails. The ring vortices, discussed in § 3 together with the positions of the wings shedding them, make clear the relation between the efficiency and the position of the axis of the pitching motion.

In § 2 the lifting-surface approach to unsteady wing theory is outlined and a mathematical formulation of the problem is made, giving formulae for the rate of working, the thrust, the propulsive efficiency, the circulation distribution in the wake, etc. These are evaluated numerically for various tail forms in § 3. In the final section, the drag coefficient C_D of the fast-swimming animals is estimated, using some observed data and the computed thrust. The results show some

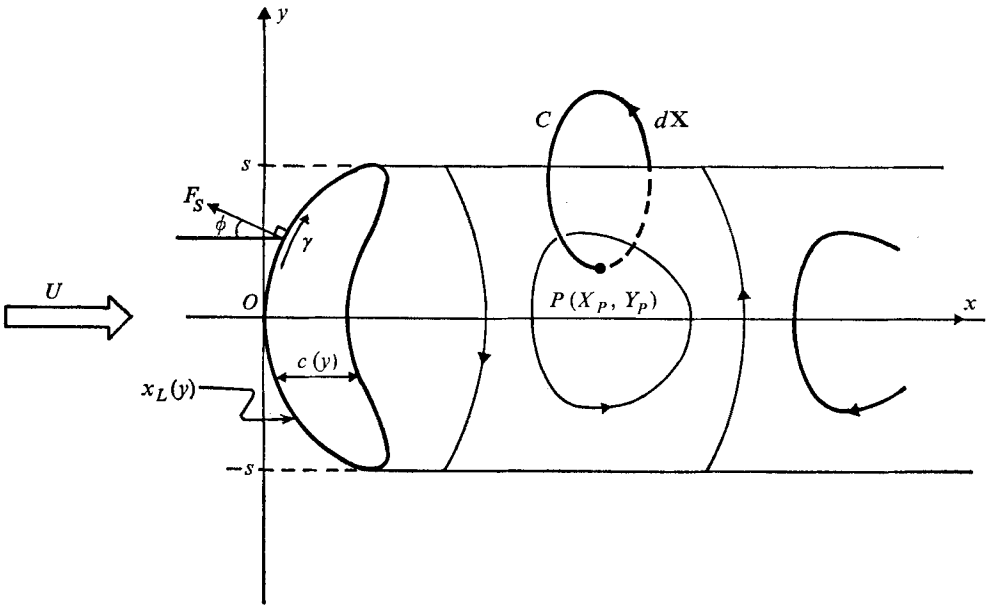

FIGURE 1. Definition sketch.

evidence of differences between the C_D's for cetacean mammals and scombroid fish respectively. These estimated drag coefficients are compared with available experimental data.

2. Mathematical formulation

In the mathematical theory of the carangiform motion of aquatic animals with lunate tails, attention is given to the motion of the caudal fin (or tail fluke in the case of cetacean mammals). This is assumed to be a plate of finite aspect ratio with a rounded leading edge and a sharp trailing edge and to be oscillating with a small amplitude in a stream of incompressible inviscid fluid of undisturbed velocity U in the $+x$ direction. The y axis is taken in a plane of the mean surface of the flat-plate wing at right angles to the x axis. The origin is taken to be the centre of the leading edge of the wing (figure 1). The z axis is normal to the x, y plane, completing a right-handed system. The wing planform is assumed to be symmetrical with respect to the x axis and to be represented by the leading-edge curve $x_L(y)$ and chord length $c(y)$, both of which are even functions of y, and by the semi-span s. The lateral displacement of the wing when oscillating with angular frequency ω is taken as

$$z = \mathrm{Re}[z_*], \quad z_* = \{h - i\alpha(x-b)\}e^{i\omega t}, \tag{1}$$

where Re means 'the real part of', h and α are real numbers signifying the amplitude of heaving and pitching motions respectively, b is the pitching axis and t time. A 90° phase difference between heaving and pitching motions is

assumed following Lighthill (1970) because any other phase difference, represented by giving an imaginary part to h, is equivalent to a change in b.

For an aerofoil oscillating harmonically with small amplitude, the linear theory of potential flow around the aerofoil and its vortex wake is fully described by Davies (1963) but is outlined here very briefly in order to facilitate the following mathematical formulation. The vortex wake shed by the wing is planar and parallel to the mainstream flow in the linear theory. The wing and its wake are replaced by a doublet sheet. The strength of the sheet is adjusted such that no loading is sustained by the wake and such that the lateral velocity $\partial\phi(X, Y, Z)/\partial Z$ of fluid at the wing (where $\phi(X, Y, Z)$ is a velocity potential in a co-ordinate system (X, Y, Z) stationary with respect to the mainstream flow, with $X = x - Ut$, $Y = y$ and $Z = z$) is equal to the velocity of lateral pushing $w = \partial z/\partial t + U\partial z/\partial x$ by the wing. Corresponding to the pushing velocity w (called the upwash velocity by Davies 1963), there is a wing loading $L(x, y, t)$, i.e. a lift force per unit area at the point (x, y) of the wing. Finally an integral equation relating the upwash velocity w and the loading L is obtained:

$$w(x, y, t) = \frac{1}{4\pi\rho U}\iint_S L(x_0, y_0, t)\, K(x - x_0, y - y_0)\, dx_0\, dy_0, \tag{2}$$

where

$$K(x, y) = e^{-i\omega x/U}\int_{-x}^{\infty} e^{-\omega\chi/U}\frac{d\chi}{(\chi^2 + y^2)^{\frac{1}{2}}},$$

S is the wing area and ρ the fluid density.

We normalize lengths and time by l (a typical length of the wing) and l/U respectively, and retain the same notation for the normalized quantities except that $\epsilon = h/l$ signifies the smallness of the amplitude of the oscillation. The wing displacement (1) is rewritten here as

$$z_* = \epsilon l \sum_{k=1}^{2} a_k \zeta_k(x)\, e^{i\nu t}, \tag{3}$$

where $\zeta_1 = 1$, $\zeta_2 = x$, $a_1 = 1 + i\theta\nu b$, $a_2 = -i\theta\nu$,

$\nu = \omega l/U$ (reduced frequency), $\theta = U\alpha/\omega h$ (feathering parameter).

The feathering parameter θ is expected to be less than 1 for significant positive thrust, and $\theta = 0$ corresponds to no pitching motion. The loading is given by

$$\begin{aligned} L(x, y, t) &= p(x, y, -0, t) - p(x, y, +0, t) \\ &= \epsilon\rho U^2 \sum_{k=1}^{2} a_k \lambda_k(x, y)\, e^{i\nu t}. \end{aligned} \tag{4}$$

Thus the integral equation (2) becomes

$$W_k(x, y) = \frac{1}{4\pi}\iint_S \lambda_k(x_0, y_0)\, K(x - x_0, y - y_0)\, dx_0\, dy_0, \tag{5}$$

where

$$W_k = \partial\zeta_k/\partial x + i\nu\zeta_k.$$

In order to solve this equation numerically for a given upwash velocity W_k, a set of $n \times m$ points $P_{ij}(x_{ij}, y_j)$ $(i = 1, \ldots, n;\ j = 1, \ldots, m)$, at which the values of

the loading $\lambda_k(x_{ij}, y_j)$ or $l_{ij}^{(k)}$ are to be determined, are chosen at the outset. The loadings $l_{ij}^{(k)}$ at these points are regarded as unknown constants to be determined. The loading function $\lambda_k(x, y)$ is then represented approximately in terms of the $m \times n$ unknown values $l_{ij}^{(k)}$ so that the exact value of $l_{ij}^{(k)}$ at P_{ij} may be obtained by use of interpolation functions which have the same behaviour as the correct loading distribution at the leading and trailing edges (see appendix A). In this way a set of simultaneous equations for $l_{ij}^{(k)}$ is set up in terms of the values of the known upwash at the upwash points, which are equal in number to the loading points but not necessarily at the same positions.

The numerical procedure has been programmed in FORTRAN by Davies (1976) and was available for our project through his kind offer.

Once the loading distribution is known, we can derive the physical quantities in which we are interested. During oscillating motion the wing does work at a rate E, with mean $\bar{E}$, and generates a thrust P, with mean $\bar{P}$, which is required to overcome the drag of the animal when swimming with velocity U. The hydromechanical propulsive efficiency η is defined by $U\bar{P}/\bar{E}$. Using (3) and (4), the rate of working of the wing is

$$\begin{aligned} E &= \iint_S \mathrm{Re}\left[\frac{\partial z_*}{\partial t}\right] \mathrm{Re}\,[-L]\,dx\,dy \\ &= \tfrac{1}{2}\rho U^3 l^2 \epsilon^2 (A_E + C_1 \cos 2\nu t + C_2 \sin 2\nu t), \end{aligned} \tag{6}$$

where

$$\left.\begin{aligned} A_E &= -\nu\,\mathrm{Im}\left[\sum_{j=1}^{2}\sum_{k=1}^{2} a_j^* a_k Q_{jk}\right], \\ C_2 + iC_1 &= \nu \sum_{j=1}^{2}\sum_{k=1}^{2} a_j a_k Q_{jk}, \quad Q_{jk} = \iint_S \zeta_j(x)\,\lambda_k(x, y)\,dx\,dy, \end{aligned}\right\} \tag{7}$$

Im means 'the imaginary part of' and a_j^* is the complex conjugate of a_j. A minus sign has been added to L, which is the force per unit area exerted by the surrounding fluid. The Q_{jk} $(j, k = 1, 2)$ are computed automatically by using the Davies program. Here we are interested not only in the mean $\bar{E}$ but also in the time variation of E, which might show a phase of negative E. In fact, work of biophysicists showing that muscle can only release positive energy whether the animal is performing positive or negative work made it important to estimate whether or not the total work done during the swimming cycle includes a phase of negative working as this would involve an additional positive energy cost.

In the two-dimensional case, we have an explicit corresponding formula for the rate of working in terms of a reduced frequency $\sigma = \omega a/U$, the feathering parameter and the position of the pitching axis with half-chord a (appendix B).

As an indicator of a negative phase of E, we define μ as the ratio of negative work to positive work:

$$\mu = |S_-|/S_+,$$

where

$$S_- = 2A_E(\pi - \psi_0) + 2(C_1^2 + C_2^2)^{\frac{1}{2}} \sin\psi_0, \quad S_+ = 2\pi A_E - S_-, \tag{8}$$

and

$$\psi_0 = \cos^{-1}[-A_E(C_1^2 + C_2^2)^{-\frac{1}{2}}].$$

Here S_- and S_+ are the negative and positive areas, respectively, enclosed by the t axis and the curve $A_E + C_1 \cos 2\nu t + C_2 \sin 2\nu t$, obtained from (6).

The total forward thrust P results from the loading L acting on the wing surface, which is inclined at an angle $\alpha \sin \nu t$ to the x axis, and the suction force acting on the rounded leading edge owing to the low pressure associated with the fast flow around it. The contribution P_L from the loading L is given by

$$P_L = \iint_S \mathrm{Re}[L]\,\alpha \sin \nu t \, dx\, dy,$$

whose mean value is

$$\bar{P}_L = \tfrac{1}{2}\rho U^2 l^2 \epsilon^2 A_L, \tag{9}$$

where

$$A_L = -\theta\nu \,\mathrm{Im}\left[\sum_{k=1}^{2} a_k Q_{1k}\right]. \tag{10}$$

The suction force, on the other hand, can be derived from the asymptotic form of the fluid velocity, which is proportional to $x_n^{-\frac{1}{2}}$ as $x_n \to 0$, where x_n is the normal distance from the leading-edge curve $x_L(y)$. This behaviour is represented in the interpolation formula for L in appendix A. At the leading edge the vortex line on the wing is parallel to the leading edge since the mainstream is assumed to be a potential flow. Accordingly the strength γ of the vortex at a spanwise position y is given by the equation

$$\rho U \gamma \cos\phi = L(x, y, t) \quad \text{as} \quad x \to x_L(y), \tag{11}$$

where ϕ is the angle between the normal to the leading edge and the x axis (figure 1). The local velocity induced by the vortex is

$$\begin{aligned} u_\gamma &= \tfrac{1}{2}\gamma = \tfrac{1}{2}L/\rho U \cos\phi \\ &= \frac{\epsilon U}{2\cos\phi} e^{i\nu(t-x_L)} G(x_L, y) \left(\frac{c(y)\cos\phi}{x_n}\right)^{\frac{1}{2}} \quad \text{as} \quad x \to x_L(y) \end{aligned} \tag{12}$$

by using (11), (4) and (A 1); here

$$\left.\begin{aligned} G(x_L, y) &= \sum_{k=1}^{2} a_k \sum_{i=1}^{2} \sum_{j=1}^{2} l_{ij}^{(k)} f_i^{(n)}(0)\, g_j^{(m)}(\eta), \\ f_i^{(n)}(\xi) &= h_i^{(n)}(\xi)\,[\xi/(1-\xi)]^{\frac{1}{2}}. \end{aligned}\right\} \tag{13}$$

Instantaneously the local suction force takes the well-known steady-flow value obtained by the Blasius theorem, by analogy with the two-dimensional case, and the mean suction force $\bar{F}_s$ per unit length of the leading edge, directed along the outward normal to the leading edge, is given by

$$\bar{F}_s = \tfrac{1}{2}\pi\rho \left[\frac{\epsilon U}{2}\left(\frac{lc(y)}{\cos\phi}\right)^{\frac{1}{2}}\right]^2 |G(x_L, y)|^2 \tag{14}$$

from the asymptotic behaviour (12) see (Lighthill 1970, § 5). The component $\bar{P}_s$ of the mean leading-edge suction along the $-x$ axis is

$$\bar{P}_s = \int_x \bar{F}_s (\cos\phi)\, l\, d\chi = \int_{-s}^{s} \bar{F}_s\, l\, dy, \tag{15}$$

where $d\chi$ is a dimensionless length of line element along the leading edge. Substitution of (14) into (15) yields

$$\bar{P}_s = \tfrac{1}{2}\rho U^2 l^2 \epsilon^2 A_s, \tag{16}$$

where

$$A_s = \tfrac{1}{4}\pi \int_{-s}^{s} c(y)\,[1 + x_L'^2(y)]^{\frac{1}{2}}\,|G(x_L, y)|^2\,dy. \tag{17}$$

Thus the total mean thrust $\bar{P}$ and the efficiency η are given by

$$\bar{P} = \bar{P}_L + \bar{P}_s = \tfrac{1}{2}\rho U^2 l^2 \epsilon^2 A_P, \quad A_P = A_L + A_s, \tag{18}$$

and

$$\eta = U\bar{P}/\bar{E} = A_P/A_E. \tag{19}$$

A dimensionless representation of the thrust is given by a coefficient defined by

$$C_T = \bar{P}/(\tfrac{1}{2}\rho U^2 \epsilon^2 S) = A_P l^2/S, \tag{20}$$

where S is the wing area. The thrust contribution from the leading-edge suction is represented by the ratio

$$\gamma_s = \bar{P}_s/\bar{P} = A_s/A_P. \tag{21}$$

We are interested in this since a very high leading-edge suction leads to boundary-layer separation, which causes a considerable thrust reduction.

It may be interesting to calculate the wake vortex pattern, which is closely related to the propulsive thrust and to the rate of expenditure of wasted energy. Knowing the distribution of circulation in the wake, we can draw vortex lines by tracing fixed values of the circulation. It is assumed that the vortex lines in the wake stay at the original position where they were shed from the trailing edge; in other words, the movement of a wake vortex, self-induced or induced by other vortices in the wake or on the wing, is neglected. Accordingly, we consider a stationary wake consisting of a vortex in the co-ordinate system (X, Y, Z) fixed to the mainstream flow. The circulation K_C around a closed curve C around the vortex wake from the negative to the positive side of a point $P(X_P, Y_P)$ (figure 1) is given by the line integral of the gradient of the velocity potential $\phi(X, Y, Z)$ along C:

$$K_C = \oint (\nabla\phi).d\mathbf{X} = \phi(X_P, Y_P, +0) - \phi(X_P, Y_P, -0).$$

Equations (179) and (186) of Davies (1963) yield

$$K_C(X_P, Y_P) = \frac{1}{\rho}\int_{t_L}^{t} L(X_P, Y_P, \tau)\frac{l}{U}\,d\tau,$$

where t_L is the time when P passed the leading edge $x_L(Y_P)$. The circulation K_C is found to be independent of time t when $t > t_T$, t_T being the time when P passed the trailing edge, because L vanishes in the wake. By using the expression for L in appendix A, we obtain the dimensionless circulation:

$$\Gamma(X_P, Y_P) = \frac{K_C}{\epsilon U l} = \exp(-i\nu X_P)\sum_{k=1}^{2} a_k \int_{x_L(Y_P)}^{x_L(Y_P)+c(Y_P)} e^{i\nu x}\lambda_k(x, Y_P)\,dx, \tag{22}$$

showing a sinusoidal dependence on X_P with period $2\pi/\nu$.

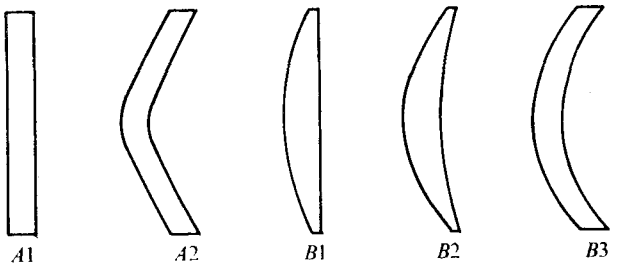

FIGURE 2. Wing planforms for which detailed calculations have been made.

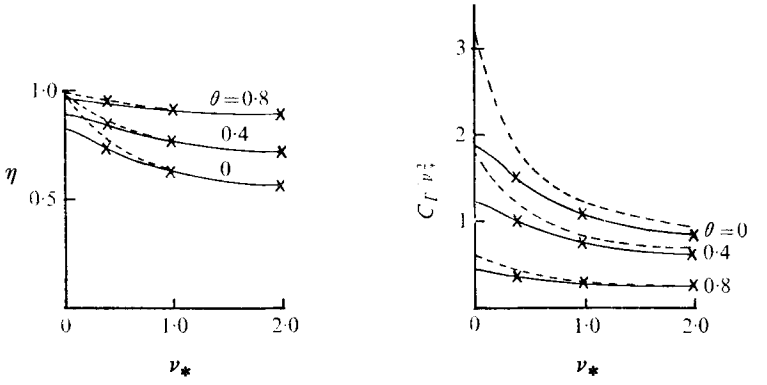

FIGURE 3. Comparison of the values of η and C_T/ν_*^2 given by the present (solid lines) and Chopra's (1974) (crosses) calculations for a rectangular wing with $\mathscr{A} = 8$. – – –, curves for a two-dimensional wing.

3. Numerical results

Using Davies' program, for given m, n and reduced frequency ν, we first calculated the loading coefficients $l_{ij}^{(k)}$ from (5) and (A 2) and the generalized force coefficients Q_{jk} from (7) for a given wing planform with a specified leading-edge curve $x_L(y)$, chord $c(y)$ and semi-span s (thus the aspect ratio $\mathscr{A}$ is defined as $4s^2/S$, where S is the wing area); these were used in the next step to obtain the three coefficients A_E, C_1 and C_2 of E from (7) and the two coefficients A_L and A_s of $\bar{P}$ [see (18)] from (10) and (17), respectively, for a given feathering parameter θ and a given position b of the pitching axis. Thus we found η from (19), C_T from (20), γ_s from (21) and μ from (8). Finally we calculated the circulation Γ from (22), enabling us to draw vortex lines in the wake. All the computations have been made with $m = 16$ and $n = 6$, giving a total number of collocation points of 96.

In order to get some idea of the accuracy of the present computation, we employed a rectangular wing with aspect ratio $\mathscr{A} = 8$ ($A1$ in figure 2), for which a computation had been made by Chopra (1974) using a completely different approach. For this wing the typical length l is taken to be the full chord c_*. Figure 3 compares the dependence of the thrust coefficient C_T/ν_*^2 and the efficiency η on θ and $\nu_* = \omega c_*/U$ for $b_* = 0{\cdot}75$ (solid lines) with that from

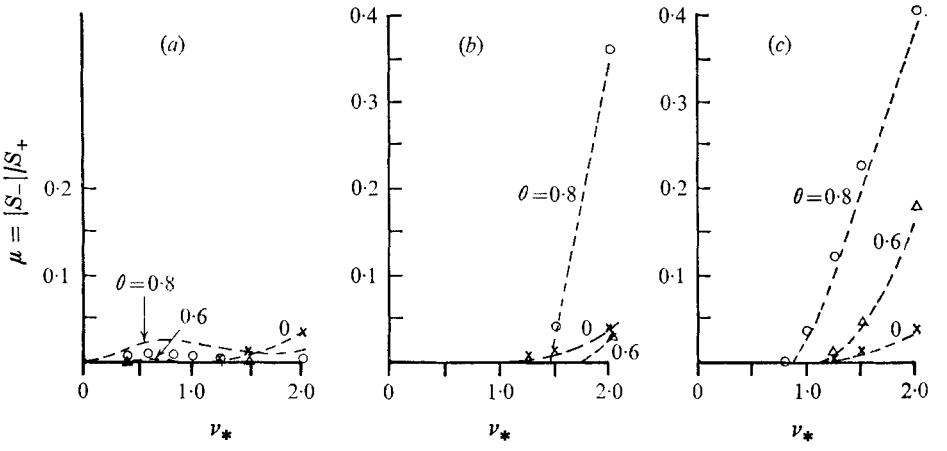

FIGURE 4. The ratio μ of negative to positive working of a rectangular wing with $\mathscr{A} = 8$. (*a*) $b_* = 0{\cdot}5$, (*b*) $b_* = 0{\cdot}75$, (*c*) $b_* = 1{\cdot}0$. ○, $\theta = 0{\cdot}8$; △, $\theta = 0{\cdot}6$; ×, $\theta = 0$; – – –, results for a two-dimensional wing.

Chopra's computation (crosses), showing fairly good agreement between them. The asterisk in ν_* and b_* means that $l = c_*$. In the same figure the performance of the two-dimensional wing calculated by Lighthill (1970) is indicated by broken lines.

Figure 4 shows the dependence of the ratio μ of the same wing on ν_* for three positions b_* of the pitching axis, as well as the μ of the two-dimensional wing (broken lines). It is found that there can be no negative work for smaller ν_* and $0{\cdot}75 \leqslant b_* \leqslant 1{\cdot}0$. Hence in both cases the wing does not do any negative work if the optimum position of pitching axis is taken ($b_* = 0{\cdot}8$ with $\theta = 0{\cdot}8$ and $\nu_* \leqslant 1$). This conclusion that lunate-tail swimming is performed under conditions which maintain a positive rate of working throughout the cycle is of clear physiological importance.

In order to find out the effect of the sweepback angle of wings on η and C_T, we took two sets of wings: one is a set (A) of sweptback wings with constant chord and the other a set (B) of parabolic wings with tapering. The first set (A) is a one-parameter family of wings (with parameter k) described by

$$c = c_*, \quad x_L = \begin{cases} k(|y| - \frac{1}{2}y_0)/s, & y_0 \leqslant |y| \leqslant s, \\ ky^2/(2y_0 s), & |y| < y_0, \end{cases} \tag{23}$$

with given c_* and y_0. All the members of the family A have the same wing area $S = 2sc_*$ and the same aspect ratio $\mathscr{A} = 2s/c_*$. In the wing shape of family A, the outboard straight (linear) leading edge is connected to the inboard parabolic one by a continuous tangent at y_0 (> 0) in order to avoid any singularity when $y_0 = 0$. We always took $s = 3$, $c_* = 0{\cdot}75$ and $y_0 = 0{\cdot}75$, yielding $S = 4{\cdot}5$ and $\mathscr{A} = 8$. Wings $A1$ and $A2$ in figure 2 correspond to $k = 0$ and $\frac{3}{2}$ respectively. Computations were made for $0 \leqslant k \leqslant 3$ and $b_* \leqslant 4$ with fixed values $\theta = 0{\cdot}8$ and $\nu_* = 0{\cdot}8$. The efficiency curves for the three fixed values $C_T = 0{\cdot}3$, $0{\cdot}5$ and $0{\cdot}7$ are shown against the sweepback angle $\phi = \tan^{-1}(k/s)$ in figure 5 (*a*).

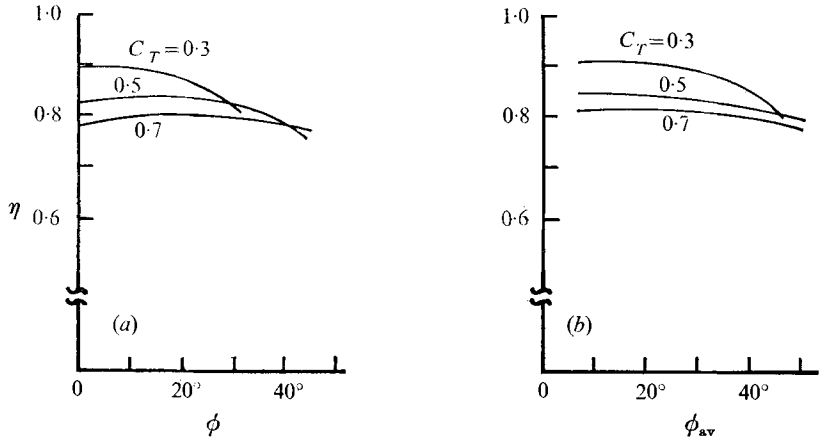

FIGURE 5. Variation of efficiency for $C_T = 0{\cdot}3$, $0{\cdot}5$ and $0{\cdot}7$. (*a*) A-wings, showing variation with the sweepback angle $\phi = \tan^{-1}(k/s)$; $\theta = 0{\cdot}8$, $\nu_* = 0{\cdot}8$. (*b*) B-wings, showing variation with $\phi_{av} = \tan^{-1}(K/s)$; $\theta = 0{\cdot}8$, $\nu_* = 0{\cdot}8$.

The wings in the second one-parameter family (B), with parameter K, are described by

$$c = c_0[1-(y/s)^2]+c_1(y/s)^2, \quad x_L = K(y/s)^2, \quad |y| \leqslant s, \tag{24}$$

with given central chord c_0 and tip chord c_1. The leading and trailing edges, i.e. x_L and x_L+c, are represented by two different parabolic curves, generating a tapering wing with area $S = \frac{2}{3}s(2c_0+c_1)$ and aspect ratio $\mathscr{A} = 6s/(2c_0+c_1)$. We always took $s = 3$, $c_0 = 1{\cdot}0$ and $c_1 = 0{\cdot}25$, yielding the same values $S = 4{\cdot}5$ and $\mathscr{A} = 8$ as for the A-wings, hence we find that the mean chord of the B-wings is $\bar{c} = 0{\cdot}75 = c_*$. Wings $B1$ and $B2$ in figure 2 correspond to $K = \frac{3}{4}$ and $\frac{5}{4}$ respectively. Computations were made for $0{\cdot}735 \leqslant K \leqslant 3{\cdot}75$ and $b_0 \leqslant 3$ with fixed $\theta = 0{\cdot}8$ and $\nu_0 = 0{\cdot}8$, where the suffix zero means that $l = c_0$. The efficiency curves for $C_T = 0{\cdot}3$, $0{\cdot}5$ and $0{\cdot}7$ are plotted against an average sweepback angle ϕ_{av} defined by $\tan^{-1}(K/s)$ in figure 5(*b*).

It is found that maximum efficiency occurs somewhere between $\phi = 0$ and 20°, depending on C_T, for A-wings and around $\phi_{av} = 14°$ (corresponding to wing $B1$) for B-wings and then the efficiency decreases with increasing sweep angle (ϕ or ϕ_{av}). Note that this result has been obtained for fixed values of θ and ν_* (or ν_0), while overall performance of the wings may be considered only by taking into account the dependence of η and C_T on θ and ν.

Wing performance has been computed in detail for the five whownings s in figure 2, the last one ($B3$) being represented by $c = 0{\cdot}75c_0$ and $x_L = K(y/s)^2$ with $K = 1{\cdot}25$. The trailing edges of $A1$ and $B1$ are straight. Some spanwise variation of the chord is given to $B1$ and $B2$ and the leading-edge curves of $B2$ and $B3$ are the same. The leading-edge curve of $A2$ is similar to that of $B2$ and $B3$ since $x_L(s = 3) = \frac{21}{16}$ for $A2$ while $x_L(s = 3) = \frac{20}{16}$ for $B2$ and $B3$. However, the partially straight leading edge of $A2$ leads to larger curvature at the centre than that of $B2$ and $B3$. We may expect to obtain some idea of the combined effect of a curved leading edge and tapering by comparing the wing performance of $A1$

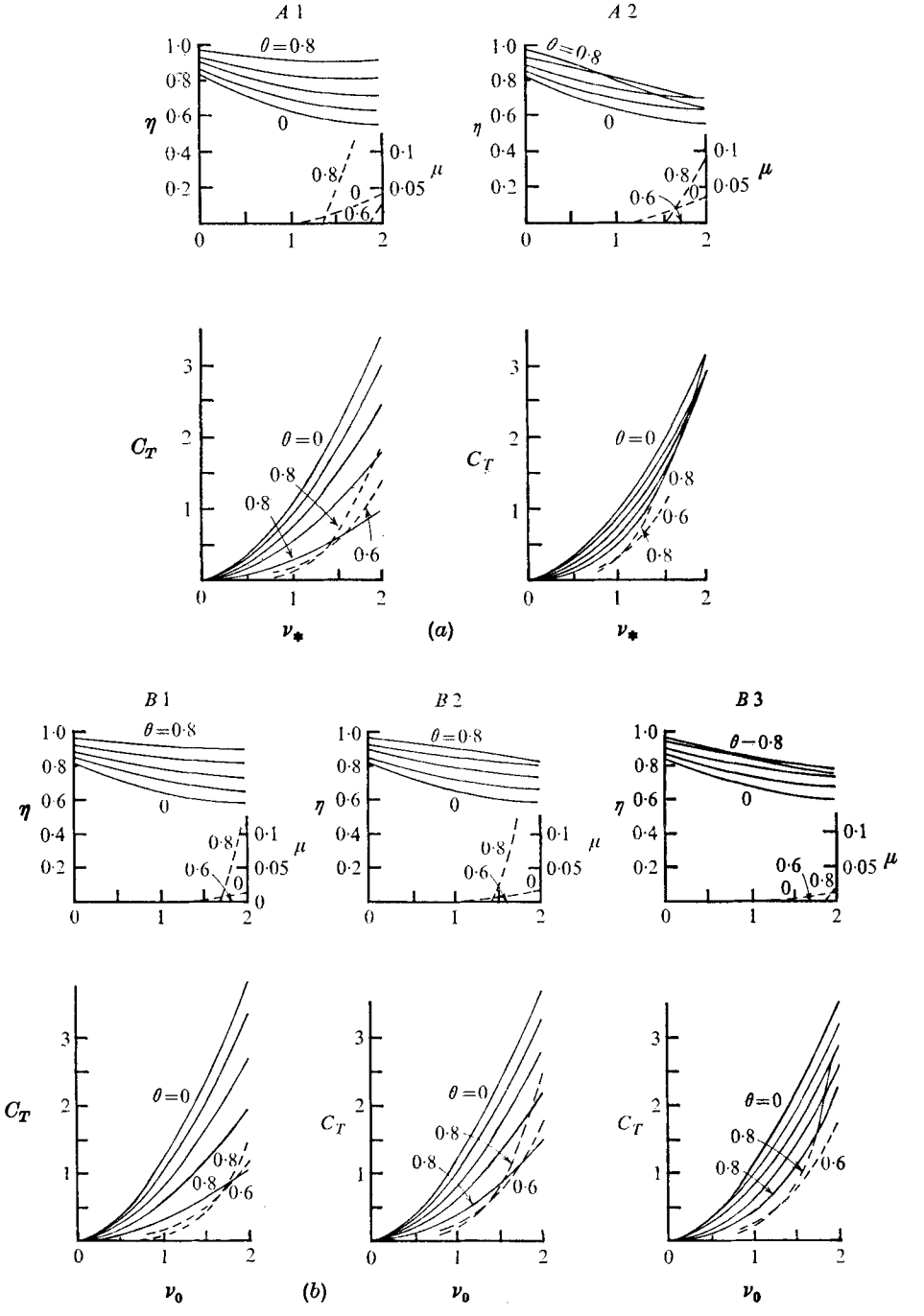

FIGURE 6. Typical η, ν and C_T, ν diagrams for (*a*) $A1$ ($b_* = 0{\cdot}75$) and $A2$ ($b_* = 1{\cdot}5$) and (*b*) $B1$ ($b_0 = 0{\cdot}8$), $B2$ ($b_0 = 1{\cdot}0$) and $B3$ ($b_0 = 1{\cdot}0$). The broken curves in the (upper) η, ν diagram show μ for $\theta = 0$, $0{\cdot}6$ and $0{\cdot}8$, while the broken curves in the (lower) C_T, ν diagram show the part of C_T coming from the leading-edge suction for $\theta = 0{\cdot}6$ and $0{\cdot}8$. (Of course C_T comes entirely from the leading-edge suction for $\theta = 0$.)

and $B1$ and also some idea of the effect of sweepback by comparing $A1$ and $A2$ or $B1$ and $B2$. Some tapering effects will be indicated by comparison between $B2$ and $B3$. The difference between $A2$ and $B3$ will show the effect of the leading-edge curvature at the centre.

Figure 6 (a) shows examples of conditions giving fairly good performance of wing $A1$ with $b_* = 0{\cdot}75$ and wing $A2$ with $b_* = 1{\cdot}5$ for $\theta = 0$, $0{\cdot}2$, $0{\cdot}4$, $0{\cdot}6$ and $0{\cdot}8$. (Reasons for the choice of particular, 'optimized' positions b_* of the pitching axis will become clear later; see figure 7.) The two broken lines in the lower (C_T, ν_*) diagram show the part of the thrust coming from the leading-edge suction for $\theta = 0{\cdot}6$ and $0{\cdot}8$. The broken curves in the upper (η, ν_*) diagram show the ratio μ of negative to positive work, with the scale on the right-hand side. The same sort of plot is shown in figure 6 (b) for wing $B1$ with $b_0 = 0{\cdot}8$, wing $B2$ with $b_0 = 1{\cdot}0$ and wing $B3$ with $b_0 = 1{\cdot}0$, the reference length this time being c_0.

We find marked differences between the η and C_T curves for $A1$ and $A2$ respectively. For $\theta = 0{\cdot}6$ or $0{\cdot}8$, the efficiency of $A2$ becomes remarkably reduced for $\nu_* > 1$, while the C_T curves for $A2$ are steeper than those for $A1$. The same sort of difference is found between $B1$ and $B3$ or $B2$ and $B3$. Hence we may say that at the cost of efficiency the sweptback wings with constant chord, like $A2$ and $B3$, can produce more thrust with the same frequency or the same increment in frequency than the rectangular wing $A1$ or tapered wings like $B1$ or $B2$. The difference in performance between $B1$ and $B2$ is smaller, but we find that the efficiency of $B2$ for $\theta = 0{\cdot}8$ decreases more rapidly than that of $B1$ for $\nu_0 > 1$, while the C_T curve of $B2$ is a little steeper than that of $B1$. It may be worth noticing that no marked difference between $A1$ and $A2$ or $B1$, $B2$ and $B3$ is found with regard to η and C_T for $\theta = 0$, $0{\cdot}2$ and $0{\cdot}4$, and hence that wing performance for smaller θ is insensitive to the wing shape. (Of course, these lower values of θ are not observed in nature, and we can see that this is due to the low efficiencies involved as well as the likelihood of boundary-layer separation resulting from the high leading-edge suction.) Conversely the performance for the observed higher values of θ (less than 1) is very sensitive to the wing shape.

The present computations of the propulsive performance of the five wings are summarized in figures 7 (a) ($\theta = 0{\cdot}8$) and (b) ($\theta = 0{\cdot}6$) for $C_T = 0{\cdot}2$, $0{\cdot}5$ and $1{\cdot}0$. Figure 7 shows the great importance of the choice b_* (or b_0) of pitching-axis position for obtaining high values both of the efficiency and of the thrust coefficient. In the upper part of each diagram three efficiency curves for fixed C_T are plotted as solid lines, the broken line is the boundary between zero and non-zero negative work, above which negative work vanishes, and the dash–dot line shows the efficiency curve for ν_* (or ν_0) $= 1{\cdot}2$, above which the reduced frequency is smaller than $1{\cdot}2$. Normally observed reduced frequencies based on the central full chord length like c_0 are less than $1{\cdot}2$ for fast-swimming aquatic animals. The lower part of each diagram shows the ratio of the thrust due to leading-edge suction to the total thrust for the same values of C_T. The wing planform corresponding to each diagram is illustrated above it together with a horizontal line showing the position of the pitching axis giving maximum efficiency for $C_T = 0{\cdot}2$ ($\theta = 0{\cdot}8$).

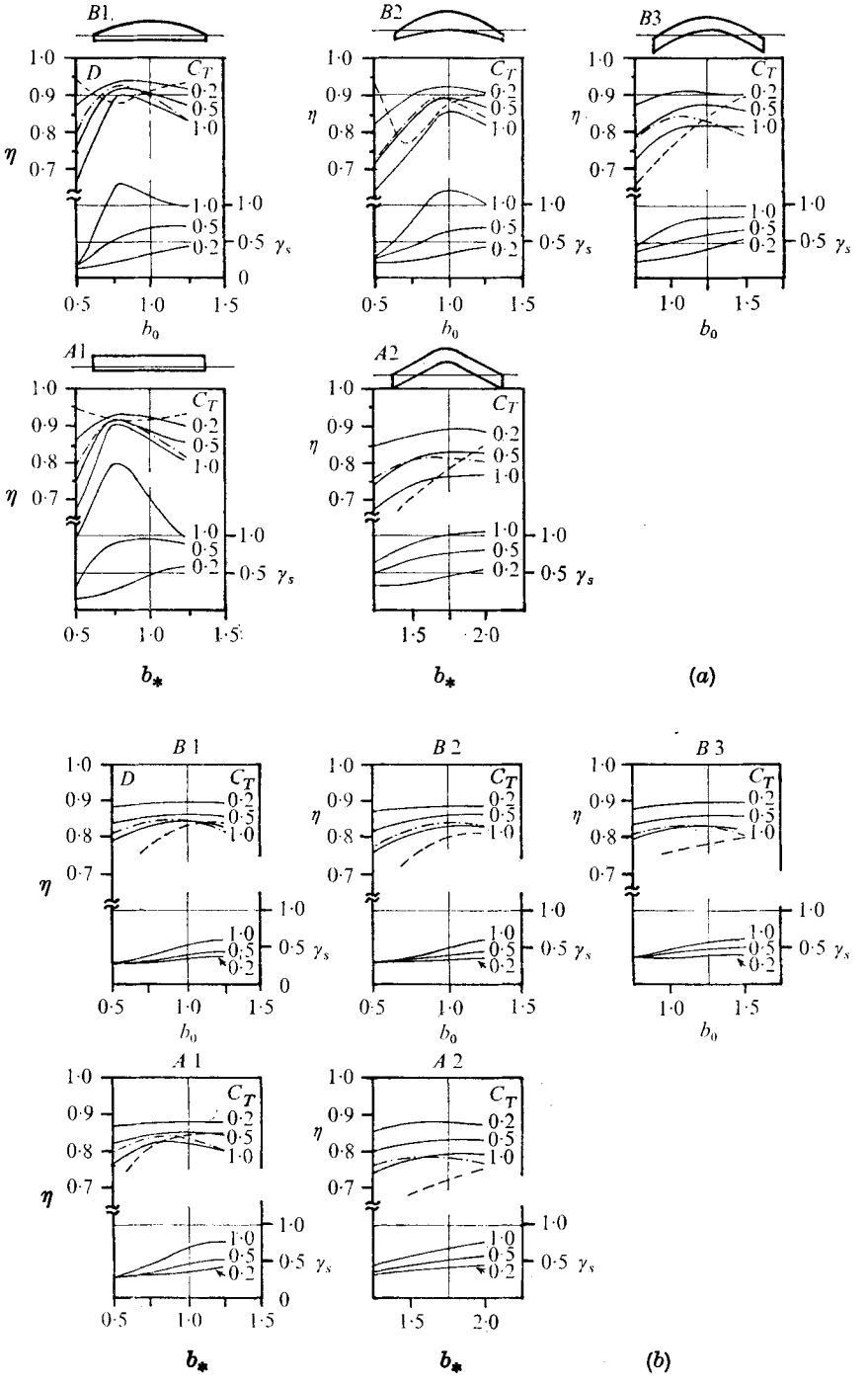

FIGURE 7. Efficiency and the ratio γ_s against b for $C_T = 0{\cdot}2$, $0{\cdot}5$ and $1{\cdot}0$ with (*a*) $\theta = 0{\cdot}8$ and (*b*) $\theta = 0{\cdot}6$. – – –, boundary between zero and non-zero negative work; — · —, efficiency curve for ν_* (or ν_0) = 1·2.

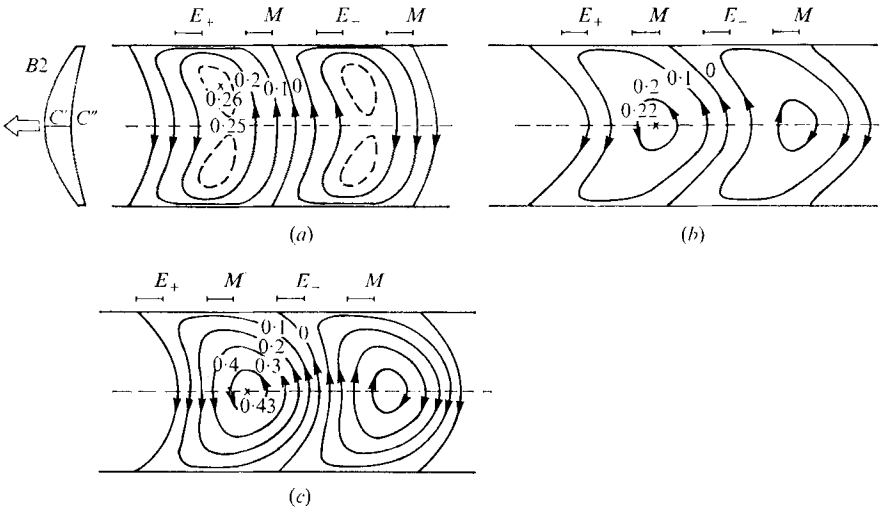

FIGURE 8. Vortex lines in the wake of wing $B2$ with $\theta = 0{\cdot}8$ and $\nu_0 = 0{\cdot}6$ for (*a*) $b_0 = 0{\cdot}5$, $\eta = 0{\cdot}876$, $A_P = 0{\cdot}558$, $C_w = A_E - A_P = 0{\cdot}080$, $\mu = 0{\cdot}039$ and $\gamma_s = 0{\cdot}19$; (*b*) $b_0 = 1{\cdot}0$, $\eta = 0{\cdot}935, A_P = 0{\cdot}622, C_w = 0{\cdot}043, \mu = 0$ and $\gamma_s = 0{\cdot}27$; (*c*) $b_0 = 1{\cdot}5, \eta = 0{\cdot}893, A_P = 0{\cdot}946$, $C_w = 0{\cdot}113$, $\mu = 0{\cdot}009$ and $\gamma_s = 0{\cdot}51$. Above each figure the four positions of the central chord $C'C''$ when the trailing edge C'' is at M, E_-, M and E_+, respectively, are shown; here $E_\pm$ signify the extreme positions of the $\pm$ sides of the oscillation and M the intermediate position.

First we consider the case $\theta = 0{\cdot}8$ (figure 7*a*). The maximum efficiency η_m for $C_T = 0{\cdot}2$ is found in the diagram for $B1$ as $\eta_m^{(0{\cdot}2)}(B1) = 0{\cdot}935$, which is not much different from $\eta_m^{(0{\cdot}2)}(A1) = 0{\cdot}930$ or $\eta_m^{(0{\cdot}2)}(B2) = 0{\cdot}925$, the difference 0·005 in η being of the order of the computational error. It is very interesting to find that all these maximum points of efficiency for $C_T = 0{\cdot}2$ lie within the region D specified by no negative working and a reduced frequency (ν_* or ν_0) less than 1·2. If we restrict ourselves to D, a thrust as high as $C_T = 0{\cdot}5$ is made possible largely by the wings $B3$ and $A2$, while no wing can generate $C_T = 1{\cdot}0$ in D with $\theta = 0{\cdot}8$. The maximum efficiency $\eta_m^{(0{\cdot}5)}$ for $C_T = 0{\cdot}5$ is found in D for $B3$; for which $\eta_m^{(0{\cdot}5)}(B3) = 0{\cdot}875$, while $\eta_m^{(0{\cdot}5)}(A2) = 0{\cdot}830$. The γ_s of all the wings for $C_T = 0{\cdot}2$ is less than 0·5 except in some cases for $A1$, $A2$ and $B3$, and is smallest for $B1$ and $B2$. However the smallest γ_s for $C_T = 0{\cdot}5$ is found for $B3$. Note that smaller γ_s is advisable for avoiding leading-edge separation.

The general impression of figure 7(*b*), $\theta = 0{\cdot}6$, is that there is little difference among the five diagrams, confirming that the performance for smaller θ becomes insensitive to the wing shape as mentioned earlier. The maximum efficiencies for $C_T = 0{\cdot}2$ and 0·5 in each diagram are all smaller than the corresponding values for $\theta = 0{\cdot}8$. However it is remarkable to find that a larger thrust ($C_T = 0{\cdot}5$) can be generated in D for $\theta = 0{\cdot}6$ by all the wings and also that an even higher thrust ($C_T = 1{\cdot}0$) is possible in D for $B3$ and $A2$. The maximum efficiency for $C_T = 0{\cdot}5$ is 0·865, found for $B1$, which is smaller than the value 0·875 for $B3$ with $\theta = 0{\cdot}8$.

Thus, if a smaller thrust ($C_T = 0{\cdot}2$) is required, the best wing out of the five

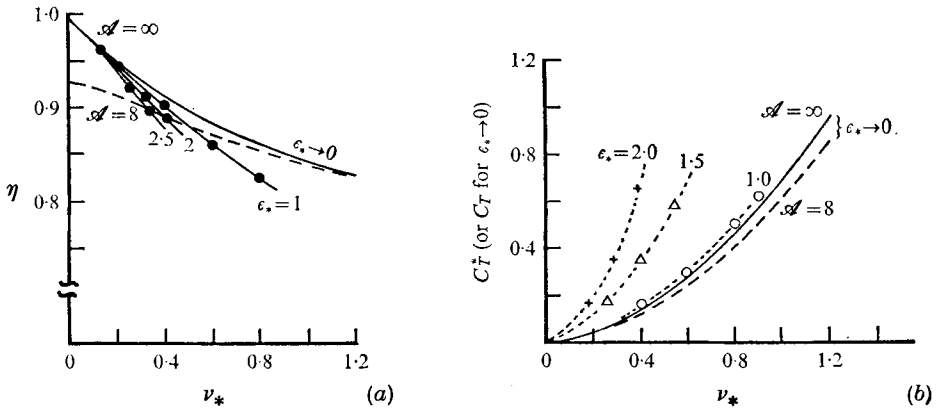

FIGURE 9. Effect of finite amplitude on (*a*) η and (*b*) $C_T^* = \bar{P}/(\frac{1}{2}\rho U^2 c_*)$. $\theta = 0{\cdot}6$.

is $B1$ with $\theta = 0{\cdot}8$. On the other hand if a thrust as high as $C_T = 0{\cdot}5$ or $1{\cdot}0$ is required, the best wing is found to be $B3$ with $\theta = 0{\cdot}8$ for $C_T = 0{\cdot}5$ and $\theta = 0{\cdot}6$ for $C_T = 1{\cdot}0$. Note that little difference is found between $B1$ and $B2$ although the overall performance of $B2$ is a little worse. As far as the efficiency is concerned, no dramatic difference is found between $B1$ and $A1$. It is important, however, that the contribution from the leading-edge suction is less for $B1$ than for $A1$, leading to a reduced likelihood of boundary-layer separation at the leading edge for $B1$, and that the maximum efficiency of $B1$ is a little higher than that of $A1$. Hence $B1$ is considered to be more advisable. As a result wings with a curved leading edge of small curvature at the centre, like the B-wings, are seen to be better than $A1$, which has a straight leading edge, or $A2$, which has a partially straight leading edge with larger curvature at the centre.

Vortex lines in the wake of wing $B2$ are illustrated in figure 8 for $\theta = 0{\cdot}8$, $\nu_0 = 0{\cdot}6$ and (*a*) $b_0 = 0{\cdot}5$, (*b*) $b_0 = 1{\cdot}0$ and (*c*) $b_0 = 1{\cdot}5$. Above each figure four positions of the central chord $C'C''$ are shown. Two of these correspond to the two extreme positions of the trailing edge C'' during lateral oscillation with $E_\pm$ signifying the extreme positions of the $\pm$ sides of $Z = 0$ respectively; the other two correspond to the intermediate position M of C'' when C'' lies in the x, y plane. The + side is supposed to be this side of the paper. Hence we can get a very rough idea of the phase of the oscillation at which the vortex ring is shed by the wing. The largest efficiency $\eta = 0{\cdot}938$ is found in (*b*), where the coefficient C_w of mean energy wastage in the wake per unit time, defined by

$$(\bar{E} - U\bar{P})/(\tfrac{1}{2}\rho U^3 c_0^2 \epsilon^2) = C_E - A_P,$$

is lowest, equal to 0·043. We can see that the centre of the wake vortex ring in (*b*) is shed when the wing is near the intermediate position M, while the corresponding centres in (*a*) and (*c*) are shifted to the left and right of M respectively. Although the largest thrust, $A_P = 0{\cdot}946$, occurs in (*c*), η is low and hence the energy wastage coefficient is comparatively large. It seems that this results from the position of shedding of the vortex ring being shifted away from the intermediate position, i.e. it is shed too early. Owing to the lower efficiency and non-zero μ [and the larger γ_s of (*c*)], cases (*a*) and (*c*) are not advisable.

4. Comparison with observations and discussion

The present results are further applied to predict the actual thrust and the associated drag coefficient of motion of aquatic animals for which some observed data are available. The results presented in the previous section have been obtained under the assumption of infinitesimal lateral oscillation. In order to make a realistic estimate of the thrust of aquatic animals, we have to extrapolate these results to finite amplitude motion. Fortunately an idea of the extrapolation may be obtained from the recent work of Chopra (1976) for finite amplitude oscillation of a two-dimensional flat plate. The specification of the wing motion by Chopra is somewhat different from the present one. However, defining an extended feathering parameter θ_* as $(U\tan\alpha)/(\omega h)$ (α should be replaced by $\theta_0-\alpha_0$ in Chopra's notation) instead of the $\theta = U\alpha/\omega h$ of the present case, we obtain the wing performance illustrated in figure 9 for $\theta_* = 0{\cdot}6$. This figure shows the amplitude effect on η and a thrust coefficient $C_T^* = \bar{P}/(\frac{1}{2}\rho U^2 c_*)$ with $\epsilon_* = h/c_*$ (c_* being the full chord, equal to $2c$ in Chopra's notation). Figures 9 (*a*) and (*b*) both show, for comparison, curves corresponding to small amplitude motion ($\epsilon_* \to 0$) of the two wings with $\mathscr{A} = \infty$ and 8 (rectangular), represented by solid and broken lines respectively. Three points on each curve for finite ϵ_* come from the three figures given by Chopra (1976). The deviation of the efficiency curves from the small amplitude case ($\epsilon_* \to 0$) becomes greater as ϵ_* increases. However, the deviations are significant only for larger values of ν_* (greater than 0·4). The deviations are most significant for still larger values of ν_* ($> 0{\cdot}6$), at which, on the other hand, the effects of finite aspect ratio are quite small. This suggests that Chopra's finite amplitude results, although calculated for the case of infinite aspect ratio, can be effectively used as a correction to our small amplitude calculations for planforms of finite aspect ratio.

Our main interest is in how the thrust depends on ϵ_*. In figure 9 (*b*) we find that C_T^* is nearly proportional to ϵ_*^2, at least up to $\epsilon_* = 2{\cdot}0$ and for $\nu_* \leqslant 0{\cdot}4$. It may be worth pointing out that the C_T^* curve for $\epsilon_* = 1{\cdot}0$ is a little above the curve of C_T ($= C_T^*/\epsilon_*^2$) for $\mathscr{A} = \infty$ and $\epsilon_* \to 0$.

In the following, two sets of data are cited: one from Fierstine & Walters (1968) on the motion of a wavyback skipjack, *Euthynnus affinis* (a scombroid fish), and the other from Wu (1971*b*) on a porpoise (or Pacific whitesided dolphin), *Lagenorhyncus obliquidens*. The data on the porpoise were first reported by Lang & Daybell (1963) (unfortunately this is not available to the authors at present). The data are summarized in table 1, which gives the body length L, speed U, Reynolds number $R = UL/\nu_{\text{vis}}$ (ν_{vis} = kinematic viscosity of water), reduced frequency ν_0, amplitude ϵ_0 and surface area ratio S_T/S_B (S_B = total body surface area, S_T = projected planform area of tail). The body length L, the central chord c_0 and the ratio S_T/S_B of the wavyback skipjack are not reported by Fierstine & Walters, so that $L = 1{\cdot}0\times10^2$ cm and $c_0/L = 6{\cdot}2\times10^{-2}$ are taken from the illustration by Masuda, Araga & Yoshino (1975). Five examples of the motion of the wavyback skipjack are shown and the maximum and minimum values are given in table 1 with the mean value in parentheses. The value of S_T/S_B for the wavyback skipjack was obtained in two steps: first, *projected*

	Body length L (cm)	Speed, U (cm/s)	$R = UL/\nu_{vis}$	$\nu_0 = \omega c_0/U$	$\epsilon_0 = h/c_0$	S_T/S_B
Porpoise	$2{\cdot}0 \times 10^2$	$5{\cdot}1 \times 10^2$	$9{\cdot}3 \times 10^6$	0·71	1·3	0·03
Wavyback skipjack	$1{\cdot}0 \times 10^2$	$3{\cdot}1$ to $8{\cdot}2 \times 10^2$ ($4{\cdot}8 \times 10^2$)	$2{\cdot}8$ to $7{\cdot}5 \times 10^6$ ($4{\cdot}3 \times 10^6$)	0·70 to 1·05 (0·94)	1·4 to 2·5 (1·9)	0·02

TABLE 1

	$B1$ ($b_0 = 0{\cdot}8$, $\theta = 0{\cdot}8$)			$B2$ ($b_0 = 1{\cdot}0$, $\theta = 0{\cdot}8$)		
	C_T	$\epsilon_0^2 C_T$	C_D	C_T	$\epsilon_0^2 C_T$	C_D
Porpoise	0·17	0·29	0·01	0·19	0·32	0·01
Wavyback skipjack	0·17 to 0·31 (0·28)	0·60 to 1·20 (0·98)	0·01 to 0·03 (0·02)	0·19 to 0·38 (0·30)	0·74 to 1·48 (1·06)	0·015 to 0·03 (0·02)

TABLE 2

surface areas S'_T ($= S_T$) and S'_B shown in a side-view photograph of the fish were measured by using a planimeter; then, the mean ratio q of the circumferential length of the cross-sections to the depth was measured for a scombroid fish bought at a fish market. The ratio S_T/S_B used in table 1 is obtained as $S_T/S'_B q$, where $q = 2{\cdot}6$. Note that the ν_0 and ϵ_0 of the porpoise correspond to the lower limit of those of the wavyback skipjack, while the R of the porpoise is higher than that of the wavyback skipjack.

In steady swimming the thrust $\bar{P} = \frac{1}{2}\rho U^2 \epsilon_0^2 S_T C_T$ is balanced by the mean total drag $\bar{D} = \frac{1}{2}\rho U^2 S_B C_D$ acting on the fish's body, yielding a drag coefficient $C_D = \epsilon_0^2 C_T (S_T/S_B)$. The tails of both the animals are assumed to be like $B1$ or $B2$. Hence estimates of C_D based on table 1 and the value of C_T for $\theta = 0{\cdot}8$ in figure 6(b) are shown in table 2. We find that the drag coefficient $C_D^{(p)}$ of the porpoise is considerably smaller than the drag coefficient $C_D^{(w)}$ of the wavyback skipjack. (The superscripts (p) and (w) refer to the porpoise and the wavyback skipjack respectively.) This smaller value $C_D^{(p)}$ resulted from the smaller $\nu_0^{(p)}$ and $\epsilon_0^{(p)}$. Note that the smallest value 0·70 of $\nu_0^{(w)}$ for the wavyback skipjack corresponds to the largest $\epsilon_0^{(w)}$, i.e. 2·5.

The value $C_D^{(p)} = 0{\cdot}01$ is larger than the C_D estimated so far for the porpoise. We are here over-estimating C_D, because thrust reduction is expected by (i) the absence of leading-edge suction over part of the tail owing to the presence of a peduncle anterior to the tail, giving an assumed reduction of 10% of the total thrust, and (ii) the smaller aspect ratio, 5·4, of the porpoise rather than the value 8 used of the present computation, leading to 6% reduction from a rough reading of the diagrams of Chopra (1974). Some substantial error must result from the assumption $\bar{P} \propto \epsilon_0^2$ for the finite amplitude motion. Thus, assuming 20% total reduction of thrust, we obtain $C_D = 0{\cdot}008$, which is still larger than the value 0·003 based on turbulent flow with 40% laminar flow around a rigid streamlined body at the speed $U^{(p)} = 2 \times 10^2$ cm/s (Wu 1971*b*). Compared with

the drag coefficient of steady swimming, the value of C_D estimated from experimental data on flow around a stationary body or from deceleration measurements during gliding is likely to be too low. For, during steady swimming, the animal is always oscillating laterally owing to recoil resulting from the tail oscillation. This is expected to lead to a value of C_D larger than 0·003. Hence the higher $C_D^{(p)}$ obtained from the computed thrust is considered to lie in the right direction. It should be noted that, if we take as the C_T in table 2 the value appropriate for $\theta = 0{\cdot}9$ instead of 0·8, the estimated values of C_D for both the animals are reduced by about half.

We must be careful about deriving anything definite from only two examples, but we are tempted to say, concerning the considerable difference between $C_D^{(p)}$ and $C_D^{(w)}$, that the flow around the wavyback skipjack might be different from that around the porpoise. In this context, two experimental measurements are referred to. The first is the frictional drag coefficient for flow along a rough flat surface, which is calculated to be 0·02, independent of R, for $L/$(dimension of roughness) = 50 by using Schlichting's semi-empirical interpolation formula (Goldstein 1938, § 168). The gills and scales on the fish's body are considered to be roughness of dimension of the order given above. The second quantity is the drag coefficient of a wing with control gaps i.e. a wing with a leading-edge slat and a trailing-edge flap. Figure 20(a) of Hoerner (1965, chap. 6) shows that $C_D = 0{\cdot}015$ ($\frac{1}{2}C_{DS}$, C_{DS} being based on the projected planform area, $C_L = 0{\cdot}3$) when there is flow through the leading-edge slat and $C_D = 0{\cdot}009$ with no flow there. This second example was chosen as we knew that, when a scombroid fish is swimming steadily, it keeps its mouth open in order to inhale a large water flow, which is exhausted as a jet through the narrow gaps of the gills. This leads to additional drag. Further, the jet from the gills may disturb the boundary layer over the fish surface, causing turbulence in it. In addition there is lateral oscillation of recoil. Therefore it seems plausible that the C_D of the wavyback skipjack (or, more generally, scombroid fishes) is as high as 0·02. This is consistent with the values 0·0085–0·025 (average 0·017) obtained from the values in table 2 by subtracting 15 %, the aspect ratio of scombroid fish being not far from 8.

Thus we may say that the flow around a porpoise is something like a turbulent flow over a smooth surface with a substantial laminar region, while the flow around the wavyback skipjack resembles flow over a rough surface influenced by through flow.

The authors are extremely grateful to Prof. Sir James Lighthill for his great help and stimulating discussion. Thanks are also due to Dr D. E. Davies, Royal Aircraft Establishment, for kindly allowing us to use his excellent computer program and for his pertinent comments. We want to thank Mrs Anne Rickett for her kindness in typing this paper. We are also grateful to the Department of Applied Mathematics and Theoretical Physics, University of Cambridge, for providing adequate facilities during the stay of both authors.

Appendix A

The loading function is written [see (4)] as

$$L = \epsilon\rho U^2 e^{i\nu t} \sum_{k=1}^{2} a_k \lambda_k(x, y), \tag{A 1}$$

where

$$\lambda_k(x, y) = e^{-i\nu x} \sum_{i=1}^{n} \sum_{j=1}^{m} l_{ij}^{(k)} h_i^{(n)}(\xi)\, g_j^{(m)}(\eta), \tag{A 2}$$

$$\xi = [x - x_L(y)]/[c(y)] = \tfrac{1}{2}(1 - \cos\theta), \quad \eta = y/s = \cos\phi, \tag{A 3}$$

$$\left.\begin{aligned} h_i^{(n)}(\xi) &= [(1-\xi)\,\xi_i/\xi(1-\xi_i)]^{\frac{1}{2}} \prod_{r=1}^{n}{}' [(\xi - \xi_r)/(\xi_i - \xi_r)] \\ &= [4 \sin \tfrac{1}{2}\theta_i/(2n+1) \sin \tfrac{1}{2}\theta] \sum_{r=0}^{n-1} \cos[(r+\tfrac{1}{2})\,\theta_i] \cos[(r+\tfrac{1}{2})\,\theta], \\ g_j^{(m)}(\eta) &= [(1-\eta^2)/(1-\eta_j^2)]^{\frac{1}{2}} \prod_{r=1}^{m}{}' [(\eta - \eta_r)/(\eta_j - \eta_r)] \\ &= [2/(m+1)] \sum_{r=0}^{m-1} \sin[(r+1)\,\phi_j] \sin[(r+1)\,\phi] \end{aligned}\right\} \tag{A 4}$$

and

$$\xi_i = \tfrac{1}{2}(1 - \cos\theta_i), \quad \theta_i = (2i-1)\,\pi/(2n+1), \quad \eta_j = \cos\phi_j, \quad \phi_j = \pi j/(m+1);$$

the dash on the product operator Π indicates that the factor with $r = i$ (or $r = j$) is to be omitted. The values of the loading function $\lambda_k(x, y)$ at the loading points (ξ_i, η_j), i.e. $l_{ij}^{(k)}$, are determined approximately by using the integral equation (5), or equivalently by a set of mn simultaneous equations obtained from it.

Appendix B. Rate of working of the two-dimensional flat-plate wing

Following Lighthill (1970, § 5), the loading is represented as $2\rho(\Phi)_{z=-0}\, e^{i\omega t}$. Hence the rate of working per unit span is given, using his notation except that b is written here as b_*, by

$$\begin{aligned} \rho E &= \int_{-a}^{a} \mathrm{Re}\,[2\rho(\Phi)_{z=-0}\, e^{i\omega t}]\, \mathrm{Re}\,[\partial Z/\partial t]\, dx \\ &= \tfrac{1}{2}\,\mathrm{Re}\,[B_1^* Z + B_2^* Q] + \tfrac{1}{2}\,\mathrm{Re}\,[(B_1 Z + B_2 Q)\, e^{2i\omega t}] \\ &= \pi a U^3 \epsilon^2 \sigma^2 (A_E + C_1 \cos 2\omega t + C_2 \sin 2\omega t), \end{aligned}$$

where

$$\begin{aligned} B_1 &= -\omega\alpha b_* + i\omega h, \quad B_2 = -\alpha\omega, \quad \sigma = \omega a/U, \\ \epsilon &= h/a, \quad \beta = b/a, \quad \theta = U\alpha/\omega h, \\ A_E &= \theta\sigma(\beta + \tfrac{1}{2})\,\psi_r - \psi_i - \sigma^2\theta^2\beta, \\ C_1 &= \theta\sigma(\beta + \tfrac{1}{2})\,\psi_r + \psi_i - \sigma^2\theta\beta(\theta - 1), \end{aligned}$$

$$C_2 = -\theta\sigma(\beta+\tfrac{1}{2})\psi_i + \psi_r - \sigma\theta + \tfrac{1}{2}\sigma[1-(\tfrac{1}{8}+\beta^2)\theta^2\sigma^2],$$

$$\psi = [\theta\sigma(\beta-\tfrac{1}{2}) + i(\theta-1)][F(\sigma)+iG(\sigma)] + \tfrac{1}{2}\theta\sigma,$$

and $F+iG$ is the Theodorsen function. It is easily shown that the constant term $\pi a U^3 \epsilon^3 \sigma^2 A_E$ is equivalent to expression (73) of Lighthill (1970).

REFERENCES

Breder, C. M. 1926 *Zoologica*, **4**, 159.

Chopra, M. G. 1974 *J. Fluid Mech.* **64**, 375.

Chopra, M. G. 1976 *J. Fluid Mech.* **74**, 161.

Davies, D. E. 1963 *Aero. Res. Counc. R. & M.* no. 3409.

Davies, D. E. 1976 *R.A.E. Tech. Memo. Structures*, no. 881. Royal Aircraft Establishment, Farnborough, Hampshire, England.

Fierstine, H. L. & Walters, V. 1968 *Mem. S. Calif. Acad. Sci.* **6**, 1.

Goldstein, S. 1938 *Modern Development in Fluid Dynamics*, vol. 2. Oxford University Press.

Hoerner, S. F. 1965 *Fluid-Dynamic Drag*. Published by the author.

Lighthill, M. J. 1960 *J. Fluid Mech.* **9**, 305.

Lighthill, M. J. 1969 *Ann. Rev. Fluid Mech.* **1**, 413.

Lighthill, M. J. 1970 *J. Fluid Mech.* **44**, 265.

Lighthill, M. J. 1971 *Proc. Roy. Soc.* B **179**, 125.

Lighthill, M. J. 1975 *Mathematical Biofluiddynamics*. Philadelphia: S.I.A.M.

Masuda, H., Araga, C. & Yoshino, T. 1975 *Coastal Fishes of Southern Japan*. Tokyo: Tokai University Press.

Wu, T. Y. 1961 *J. Fluid Mech.* **10**, 321.

Wu, T. Y. 1971*a* *J. Fluid Mech.* **46**, 337.

Wu, T. Y. 1971*b* *J. Fluid Mech.* **46**, 521.

Wu, T. Y. 1971*c* *J. Fluid Mech.* **46**, 545.

Wu, T. Y. 1971*d* *Adv. in Appl. Mech.* **11**, 1.